Synthesis, Characterization, and Antimicrobial Activity of New Metal Complexes Derived from 4-chloro-N'-[(E)-(3,5-dichloro-2-hydroxyphenyl) methylidene] benzohydrazide

Kirti P. Mhatre[1], Dipti D. Gharat[1], Shailesh A. Tawde[2], Ramesh S. Yamgar[2], Shashikant D. Ajagekar[1*]

[1]Department of Chemistry, Thakur College of Science and Commerce, Kandivali East, Mumbai, Maharashtra, India-400 101
[2]Department of Chemistry, CS's S.S. & L.S. Patkar College of Arts & Science, and V. P. Varde College of Commerce & Economics, Goregaon, Mumbai, India-400062.

***Corresponding Author:** Shashikant D. Ajagekar
Email: drsdajagekartcsc@gmail.com

ABSTRACT
Metal(II) complexes, derived from the ligand 4-chloro-N'-[(E)-(3,5-dichloro-2-hydroxyphenyl)methylidene]benzohydrazide (HCBHDCS), were synthesized. These included elemental analyses, IR, UV-VIS, ^{1}H and ^{13}C NMR, ESR and mass spectroscopy, and magnetic susceptibilities and conductivities measurements. The Fe(II), Mn(II), Cu(II), Co(II), and Mn(II) complexes exhibit a high spin octahedral geometry, Pd(II) is square planar, and Cd(II), Hg(II) and Zn(II) are tetrahedral in nature. The electron spin resonance (ESR) spectrum observed in solid copper(II) complex exhibits distinct characteristics indicative of their specific configurations. This complex possesses a ground state with an axial symmetry type. The obtained values substantiated distorted octahedral geometry, indicating a significant ionic or covalent environment. Values for molar conductance in DMF show complexes' non-electrolytic behavior. To determine their crystal structures, X-ray powder diffraction is used. Antimicrobial activity has been tested in the metal complexes and Schiff's base HCBHDCS ligand. In comparison to regular streptomycin, each combination and ligand has greater antibacterial activity against the bacteria E. Coli. At the same time, C. albicans (MCC 1439) and S. cerevisiae (MCC 1033) show good antifungal efficacy, with growth reduced by more than 90% in response to Mn(II) and Fe(II) complexes, respectively. The in-vitro cytotoxic effects of these synthesized ligands and their complexes were also investigated using the brine shrimp bioassay.

Keywords: Antimicrobial activity, Cytotoxic study, 4-chlorobenzohydrazide, 3, 5-dichlorosalicyaldehyde and octahedral geometry

1. INTRODUCTION:

Because of their biological activity, oxime-hydrazones and related coordination compounds are attracting more and more attention. Several naturally occurring compounds or their synthesized analogs have formed the basis for highly effective anticancer medicines. Metal complexes are superior antitumor agents due to their unique characteristics [1, 2]. To attach to negatively charged biological molecules, metals must first be prepared with positively charged ions in an aqueous solution [3, 4]. To generate hydrolysis reactions, metal ions' high electron affinities can dramatically polarise groups bound to them [4]. In addition, metal ions can coordinate ligands in three dimensions, enabling the functionalization of groups that can be manipulated to bind to specific molecular targets [5, 6]. Because of their biological actions as fungicides [7, 8], bactericides [9], analgesics [10, 11], antioxidants [12, 13], anticancer agents [14, 15], and insecticides [16], oximes, hydrazones, and their coordinated compounds have recently garnered much attention. According to the literature [17], metal complexes of bis-hydrazone produced from isatin-monohydrazone and 2-hydroxy-l-naphthaldehyde showed promising biological characteristics. Great cytotoxicity was observed against Artemia salina with oxovanadium (IV) complexes generated from 2-thiophene carboxylic acid hydrazide [18]. There have also been reports of oxime-type ligand-derived copper (II) and nickel(II) homo- and heteronuclear complexes with IC50 values indicating possible antioxidant activity [19]. Cobalt (II) complexes of 2-furaldehyde oximes were tested against copper complexes of furan oximes for their cytotoxicity and mode of action to see if the metal used makes a difference. It was demonstrated [20] that cytotoxicity and mechanism of action can vary depending on the metal used. When combined with metal (II) salts, oxime hydrazones can form either mono- or binuclear complexes. The ketoamide and deprotonated enolimine forms of the keto hydrazone moiety are candidates for metal coordination. Tridentate, mono- or diprotic ligands connecting through the amide oxygen, imine nitrogen, and oxime nitrogen are prevalent for compounds containing both oxime and hydrazone groups [21]. Many researchers have taken an interest in synthesizing oxime-hydrazide compounds as key target structures and assessing their biological activity. Based on these findings, researchers have been able to design molecules with novel biological properties. New metal complexes formed from 4-chloro-N'-[(E)-(3,5-dichloro-2-hydroxyphenyl)methylidene]benzohydrazide were synthesized and characterized, highlighting the interest and

significance of oxime-hydrazide complexes. The work was extended to study the antimicrobial and cytotoxic activities of the HCBHDCS ligand and its metal complexes.

2. EXPERIMENTAL:

2.1. Materials:

The HCBHDCS ligand and complex production reagents were of analytical grade and were not further purified. The BLD Pharma firm supplied the metal salts and 4-chlorobenzohydrazide. TLC verified that all chemicals were pure. The Pune University, India's microanalytical facility, examined the HCBHDCS ligand and its metal complexes for carbon, hydrogen, and nitrogen. The concentration of metal ions was calculated using volumetric estimation [21]. A Brucker FT-IR spectrophotometer was used to acquire KBr disc FT(IR) spectra of the HCBHDCS ligand and its metal complexes across the 400 to 4000 cm^{-1} wavelength range. A JASCO V650 spectrophotometer recorded 200-1000 nm electronic spectra. At room temperature, the Gouy method was used to test magnetic susceptibilities with mercurictetrathiocyanatocobaltate(II) serving as the standard. Pascal's constant [22] was used to make approximations for diamagnetic adjustments. At 25 °C, the molar conductance of a 10^{-3} M solution of the complexes in nitrobenzene was determined using a Hitech Lab India Digital Conductivity Meter. The HCBHDCS ligand, as well as its complexes with Pd(II), Zn(II), Cd(II), and Hg(II), were subjected to analysis using a Brucker 400-MHz spectrophotometer to produce their respective 1H and 13C NMR spectra. The chemical changes (expressed in parts per million) were reported concerning tetramethylsilane (TMS). ESR measurements were conducted on solid complexes at room temperature using a JES - FA200 ESR Spectrometer with X and Q bands. The mass spectra were acquired using the Bruker IMPACT HD mass spectrometer.

SYNTHESIS OF LIGAND:

A hot ethanolic solution of 3, 5-dichlorosalicyaldehyde was added dropwise to a hot 4-chlorobenzohydrazide with continual agitation (Scheme-1). For 30 min, the reaction mixture was heated in an oil bath. After chilling to room temperature, white-colored PPT was filtered, washed with ethanol, and dried under vacuum. The yield was 75.55%, and the melting point is 187 °C.

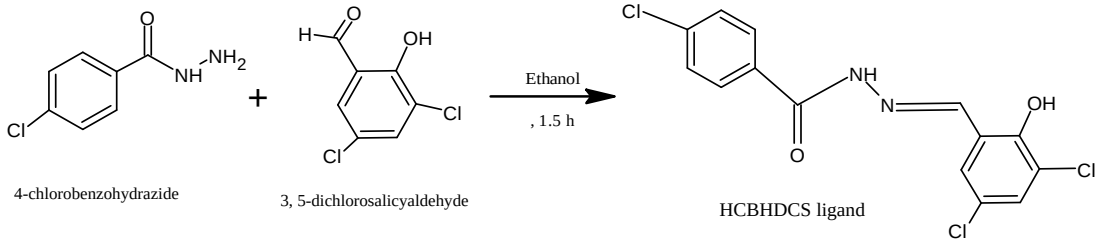

Figure 1: Preparation of HCBHDCS ligand

PREPARATION OF COMPLEXES:

A hot ethanolic solution of the appropriate metal salt (5mmol) was added to a 25 mL hot ethanolic solution of HCBHDCS ligand (10mmol) under steady stirring. The reaction took place in hot ethanol. The pH of the reaction mixture was raised to 7 by adding 0.1 N NaOH. The mixture was refluxed in an oil bath for three hours. A solid product was prepared after the resultant solution had been digested to the point where its volume had been decreased by half. The product was washed with ethanol after drying at room temperature. Yield = 71-84%.

X-RAY POWDER DIFFRACTION:

To understand more about the lattice dynamics of the compound, X-ray powder diffraction patterns were taken in the $5° < 2\theta < 90°$ positions. The X-ray powder diffraction pattern reveals only that each solid represents a distinct compound of a definite structure free of contamination from the starting materials by comparing the resulting patterns. This procedure for identifying complexes followed the standard protocol. Such evidence points to the amorphous nature of the compounds as synthesized.

BIOLOGICAL EVALUATION:

Using the standard disc-agar diffusion method, the compounds were tested for their efficacy against Gram-positive bacteria such as Staphylococcus aureus (MCC 2408), B. subtilis (MCC 2010), and Gram-negative bacteria such as Escherichia coli (MCC 2412), Pseudomonas aeruginosa (MCC 2080), as well as fungi such as Candida albicans (MCC 1439) and S cerevisiae. Fluconazole was the standard for Gram-negative bacteria. Before testing, DMSO (with no inhibitory effect) was used to dissolve the compounds into 2 and 1 mg/mL with concentrations. The experiment was carried out on a medium of 200 g of potato infusion, with concentrations

of 6g of dextrose and 15 g of agar (known as potato dextrose agar, or PDA) [23]. Filter paper disks were impregnated with 10 mL of a solution containing a predetermined concentration of test compounds and carefully placed on incubated agar surfaces. The clear zones around each disk were measured after 36 hours of incubation at 27°C for bacteria and 48 hours at 24°C for fungi.

CYTOTOXIC STUDY:

Eggs of the brine shrimp (Artemia salina Leach) were incubated in an artificial seawater solution made from a commercial salt mixture and double-distilled water in a shallow rectangular plastic plate (22x32 cm). A perforated tool was used to divide the plastic dish into two halves. The larger, darker chamber contained about 50 milligrams of eggs, while the smaller, lighter section was left open to natural light. Two days later, nauplii were pipetted from the illuminated side. We dissolved 20 mg of the test chemical into 2 ml of DMF for the sample. Nine vials were filled from stock solutions of 500, 50, and 5mg/mL (three replicates of each dilution were used for each test sample, and LD50 is the mean of three results), and one was kept as a control with 2 mL of DMF only. Overnight, the solvent was allowed to evaporate. After two days, the shrimp larvae were ready to be put into the seawater (1 mL each vial) and 10 adult shrimp (30 shrimp/dilution). The volume was then adjusted with seawater to 5 mL per vial. The final tally of surviving was taken after 24 hours [24, 25]. The LD50 values [26] were calculated using data examined by the Finney computer tool.

RESULTS AND DISCUSSION:

All complexes are soluble in ordinary organic solvents like $CHCl_3$ and, to a much greater extent, in DMF and DMSO, and they retain their colors and stability at room temperature. The hypothesized structures (**Figure 2**) are consistent with the analytical and physical findings (**Table 1**). Despite extensive efforts, no single crystals capable of producing diffractive rays have been created. The complexes are non-electrolytic since their molar conductance in 10^{-3} M nitrobenzene at 28°C are between 0.85 – 6.38 ohm^{-1} cm^2 mol^{-1} [27, 28]. The relatively high readings for several complexes suggest partial dissociation in nitrobenzene. According to the elemental studies, all complexes were produced at a molar ratio of ML_2.

Table 1: Physico-chemical and analytical data of HCBHDCS ligand and its metal complexes

Comp	Color	MW	% Yield	MP/DP	Element Content						Cond	MM
					M	C	H	N	O	Cl		
HCBHDCS	White	343.59	75.55	187	-	48.94	2.64	8.15	9.31	30.35	-	-
$Fe(CBHDCS)_2$	Blue	741.02	73.17	203	7.56	45.34	2.19	7.56	8.64	28.70	2.25	5.65
$Co(CBHDCS)_2$	Brown	746.17	82.44	196	7.91	45.03	2.17	7.51	8.58	28.50	1.68	5.02
$Ni(CBHDCS)_2$	L. Green	745.87	79.67	203	7.87	45.05	2.17	7.51	8.58	28.60	0.90	2.93
$Pd(CBHDCS_2$	Green	793.18	82.43	208	13.36	42.36	2.04	7.06	8.07	26.85	0.85	-
$Cu(CBHDCS)_2$	Green	750.73	86.97	200	8.46	44.76	2.16	7.46	8.53	28.40	1.71	2.07
$Zn(CBHDCS)_2$	Yellow	752.57	74.87	198	8.69	44.65	2.15	7.44	8.50	28.30	2.80	-
$Cd(CBHDCS)_2$	Yellow	867.18	79.34	203	14.06	42.02	2.03	7.00	8.00	27.30	6.38	-
$Hg(CBHDCS)_2$	Green	867.18	89.04	203	25.09	42.02	2.03	7.00	8.00	26.40	1.88	-
$Mn(CBHDCS)_2$	Brown	740.12	85.49	193	7.10	45.40	2.19	7.54	8.45	28.80	1.74	5.12

^{1}H NMR SPECTRA OF HCBHDCS LIGAND:

The ^{1}H NMR spectra were obtained in $CDCl_3$ and used to infer the structure of the HCBHDCS ligand; the relevant data are summarised in **Table 2**. A singlet (S, 1H) at 12.61 ppm was detected in the ^{1}H NMR spectra of the HCBHDCS ligand. The proton of the imino-NH group was identified as the singlet at 12.49 ppm (S, 1H, imino). The methyl group's lone proton has been determined to resonate as a sharp singlet (S, 1H, -CH=) with a frequency of 8.62 ppm. The indications between 7.24 and 8.037 ppm have been attributed to aromatic protons.

Table 2: ^{1}H NMR spectral data of HCBHDCS ligand and its metal complexes

Comp	-OH (C2)	-NH-	-CH=	Aromatic Protons
HCBHDCS	12.61	12.49	8.62	7.39-8.04
$Pd(CBHDCS)_2$	-	12.48	8.65	7.41-8.02
$Zn(CBHDCS)_2$	-	12.65	8.68	7.24-8.51

$Cd(CBHDCS)_2$	-	12.49	8.62	7.69-8.55
$Hg(CBHDCS)_2$	-	12.49	8.62	7.69-8.04

MAGNETIC MOMENT AND ELECTRONIC ABSORPTION SPECTRA:

The HCBHDCS ligand and its complexes were examined by measuring their electronic spectra in dimethylformamide. Information on electronic absorption spectra and magnetic moments is included in **Table 3**. This information is used to estimate the structure of synthetic transition complexes. High-energy bands were seen in the ligand's electronic absorption spectra at 235 nm (corresponding to the aromatic ring π→π* transition), 281 nm (>C=O transition), and 357 nm (n–π* transitions of C=N groups) [29]. However, in complexes where intra-ligand and LMCT transitions of coordinated ligands are responsible, these bands shift to 298-336, 265-345, and 368-425 nm, respectively [30]. One wideband at 518 nm was ascribed to the $^5T_{2g} \rightarrow {}^5E_g$ transition, confirming the octahedral geometry of the complex and yielding a magnetic moment value of 5.65 B.M. for the Fe (II) complex [31]. The magnetic moments of Co (II) and Ni(II) complexes were 5.02 and 2.93 B.M., respectively [32-33]. The d-d ($^4T_{1g}$ (F) → $^4T_{1g}$ (F) and $^4T_{2g}$ (F) → $^4T_{1g}$ (P)) transition in the Co(II) complex's electronic spectrum suggests an octahedral geometry. In contrast, the Ni(II) complex's spectra display three transitions at 972, 618, and 524 nm assignable to $^3T_{2g} \rightarrow {}^3T_{2g}$, $^3T_{2g} \rightarrow {}^3T_{1g}$(F) and $^3T_{2g} \rightarrow {}^3T_{1g}$(P), respectively [34-35]. This indicated an octahedrally warped setting. The octahedral structure of the Mn(II) complex is responsible for the appearance of the lowest energy band at 428 and 345 nm, which is a result of the d-d ($^6A_{1g} \rightarrow {}^4T_{1g}(^4P)$, and $^6A_{1g} \rightarrow {}^4E_g(^4D)$) transition [36]. Transitions at 343 and 265 nm were seen in the electronic spectra of the Pd(II) complex. A square planar geometry was attributed to these changes [37]. However, the d-d band is not present in the Zn(II), Cd(II), and Hg(II) complexes because the d^{10} transition is filled in these complexes [38-40].

Table 3: Electronic spectral data of HCBHDCS ligand and its metal complexes

Compound	λnm	Transition
HCBHDCS	357	n→π*
	281	π→π*
	235	π→π*
$Mn(CBHDCS)_2$	428	$^6A_{1g} \rightarrow {}^4T_{1g}(^4P)$
	345	$^6A_{1g} \rightarrow {}^4E_g(^4D)$
$Fe(CBHDCS)_2$	518	$^5T_{2g} \rightarrow {}^5E_g$
	425	L → M charge transfer
$Co(CBHDCS)_2$	900	$^4T_{1g(F)} \rightarrow {}^4T_{2g(F)}$ (v_1)
	668	$^4T_{1g(F)} \rightarrow {}^4T_{2g(P)}$ (v_2)
$Ni(CBHDCS)_2$	972	$^3T_{2g} \rightarrow {}^3T_{2g}$ (v_1)
	618	$^3T_{2g} \rightarrow {}^3T_{1g}$(F) ($v_2$)
	524	$^3T_{2g} \rightarrow {}^3T_{1g}$(P)
$Pd(CBHDCS)_2$	343, 265	L → M charge transfer
$Cu(CBHDCS)_2$	625	$^2B_{1g} \rightarrow {}^2A_{1g}$ (v_1)
$Zn(CBHDCS)_2$	483, 348	L → M charge transfer
$Cd(CBHDCS)_2$	368, 341, 283	L → M charge transfer
$Hg(CBHDCS)_2$	346	L → M charge transfer

FT(IR) SPECTRA:

Table 4 exhibits the results of an analysis of the IR spectral data comparing the bonding types that occur in complexes to those that occur with free HCBHDCS ligands. The free HCBHDCS ligand exhibits IR bands at 3216, 3190, and 1652 cm^{-1} for phenolic υ(C-O), υ(N-H), and υ(C=O), respectively [41-43]. The phenolic band was observed at 3216 cm^{-1} in the ligand; the absence of this band in complexes is evidence that the phenolic oxygen has been coordinated with metal ions via deprotonation [44]. This was confirmed by the fact that the phenolic υ(C-O) frequency was shifted higher, from 1301 to 1349 cm^{-1}, compared to the ligand frequency, which was shifted higher, to 1292 cm^{-1} [45-46]. The υ(C=N) stretching frequency shifted to 44-60 cm^{-1} in the metal complexes. It proves that the azomethine molecule's nitrogen is coupled to the metal ion. Lowering of the υ(C=O) vibrations in the spectra of all transition metal complexes indicates their participation in the complexation process [47-48]. The HCBHDCS ligand in metal complexes are monobasic, and this result proved tridentate. The bands observed in the far-infrared region can be attributed to the υ(M-O), υ(M-O), and υ(M-N) vibrations, respectively, at 551-625, 523-564, and 525-529 cm^{-1} [48-52].

Table 4: FT(IR) spectral data of HCBHDCS ligand and its metal complexes

Comp	-OH (C2)	-NH-	-C-H=	>C=O	>C=N-	Phenolic C-O	N→M	O→M	O-M
HCBHDCS	3216	3190	3044	1652	1605	1292	-	-	-
$Fe(CBHDCS)_2$	-	3236	3079	1600	1554	1284	604	557	527
$Co(CBHDCS)_2$	-	3398	3065	1604	1561	1301	606	550	539
$Ni(CBHDCS)_2$	-	3373	2844	1599	1557	1307	551	523	521
$Pd(CBHDCS)_2$	-	3390	3091	1643	1553	1381	621	-	535
$Cu(CBHDCS)_2$	-	3398	3068	1614	1544	1290	581	545	529
$Zn(CBHDCS)_2$	-	3384	3079	1615	1553	1312	610	-	528
$Cd(CBHDCS)_2$	-	3408	3078	1593	1549	1326	618	-	532
$Hg(CBHDCS)_2$	-	3393	3072	1651	1563	1349	564	-	510
$Mn(CBHDCS)_2$	-	3384	3073	1594	1563	1309	625	564	525

ESR SPECTRUM OF Cu(II) COMPLEX:

At room temperature, the ESR spectrum of $[Cu(CBHDCS)_2]$ is typical of a species with a d^9 configuration and an axial symmetry type of a d_{x2-y2} ground state [52]. g_{iso} = 2.17 and 2.09 indicated isotropic type, owing to tetragonal distortion [26, 33] and elongation along the fold symmetry axis Z. $G = (g_{||}-2)/(g_{\perp}-2)$ is the formula that connects the g-values. In this case, the local tetragonal axes are parallel or slightly misaligned if G > 4.0, and considerable exchange coupling is present if G< 4.0. The complex has a G value of less than 4.0, indicating the presence of tetragonal axes. Additionally, the g values for these complexes were below 2.3, indicating numerous covalent bonds surrounding the copper(II) ion [54-55]. The α-covalence parameter in the plane, $\alpha^2(Cu)$, is also included. The $[Cu(CBHDCS)_2]$ complex has a covalent bond nature, with computed values of 0.75 supporting this hypothesis [46-51]. Copper(II) complex stereochemistry is inferred from the $g_{||}/A_{||}$ ratio. The stereochemistry of the copper(II) complex may be indicated by this ratio, as postulated by Karlin [58]. For copper(II) complex with a completely square base geometry, a $g_{||}/A_{||}$ quotient in the (166-173.5) cm^{-1} range is predicted, while tetragonally deformed complexes are predicted to have a value greater than 148 cm^{-1} in contrast.

X-RAY DIFFRACTION STUDY:

The X-ray diffractogram of a Co(II) metal complex sample was analyzed within the angular range of 5-100° using a wavelength of 1.54 Å. Analysis of the diffractogram provided information on the inter-planar spacing (d-values), relative intensity, and 2θ values of each peak. Twelve reflections were observed in the diffractogram of the Co(II) complex, with the highest intensity peak occurring at 2θ = 30.35°, corresponding to a d-value of 2.93Å. An algorithm was employed to index the prominent peaks with relative intensities greater than 10%, yielding volume, unit cell characteristics, and Miller indices (hkl). The Co(II) complex unit cell exhibited lattice constants a = 8.30 Å, b = 3.14 Å, c = 6.70 Å, and a unit cell volume V = 165.29 $(Å)^3$. The criteria for monoclinic compounds, such as $a \neq b \neq c$ and $\alpha = \gamma = 90° \neq \beta$, were found to be satisfied based on these characteristics. Consequently, the crystal structure of the metal complex was determined to be monoclinic. The theoretical density of the Co(II) complex was calculated as 2.30 g cm^{-3}, while the experimental density, obtained via the specific gravity method, was measured as 2.31 g cm^{-3}. A comparison of experimental and theoretical densities indicated good agreement within the range of experimental error.

ANTIBACTERIAL BIOASSAY:

According to the literature procedure, ten different compounds were tested against four different bacterial strains (**Table 5**): two Gram-negative (*E. coli* and *P. aeruginosa*) and two Gram-positive (*S. aureus* and *B. subtilis*) [59-60]. Streptomycin standard in this field was used to evaluate the outcomes. The Pd(II) complex showed strong activity against *E. coli* and *P. aeruginosa* and moderate activity against *S. aureus* and *B. subtilis*. Similar to Mn(II), Cu(II) and Fe(II) complexes were found to be more effective against the same strains. It was fascinating to see that the bactericidal activity of these complexes (Pd(II), Mn(II), Cu(II), and Fe(II)) varied depending on whether or not the carbon chain contained methylene. The ability to kill bacteria grew along with the length of the carbon chain. The antimicrobial activity of the Co(II) complex was highly noticeable against both Gram-positive and Gram-negative bacteria. The Ni(II) complex was very active against Escherichia coli,

moderately active against B. subtilis, and weakly active against S. aureus. These ligands/complexes were also tested in vitro against the same Gram-negative and Gram-positive bacterial strains as metal complexes of cobalt (II), copper (II), nickel (II), and zinc (II). It was clear that coordination with the metal ions increased the overall potency of the uncoordinated molecules.

Table 5: Antibacterial studies of HCBHDCS ligand and its metal complexes

Compound	Antibacterial Activity (zone of inhibition) (mm)			
	S. aureus	***B. subtilis***	***E. coli***	***P. aeruginosa***
HCBHDCS	6	7	6	8
$Fe(CBHDCS)_2$	13	9	17	16
$Co(CBHDCS)_2$	12	14	12	15
$Ni(CBHDCS)_2$	7	10	18	13
$Pd(CBHDCS)_2$	15	17	18	20
$Cu(CBHDCS)_2$	11	12	16	17
$Zn(CBHDCS)_2$	16	7	13	12
$Cd(CBHDCS)_2$	12	10	8	7
$Hg(CBHDCS)_2$	21	8	9	13
$Mn(CBHDCS)_2$	8	6	13	15
Streptomycin	13	15	14	14

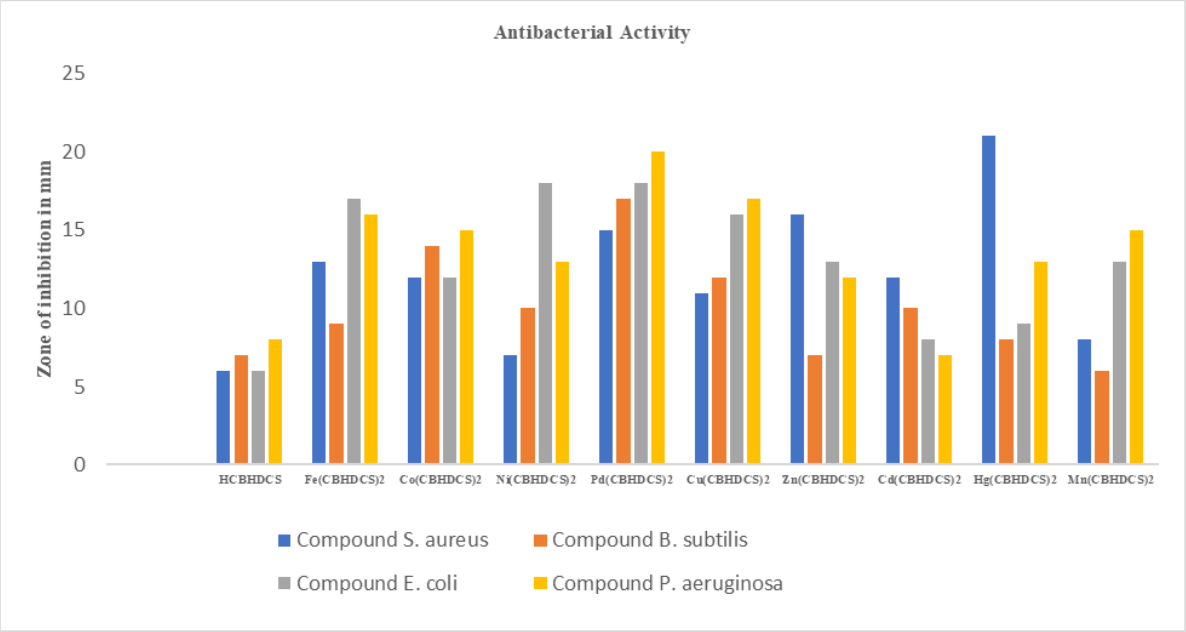

Figure 2: Antibacterial activity of HCBHDCS ligand and its metal complexes

ANTIFUNGAL BIOASSAY:

Candida albicans and Saccharomyces cerevisiae were used in an antifungal screening of all compounds using a procedure described in the literature [61]. The efficiency of fluconazole, the preferred treatment, was compared. Based on the data in **Table 6**, the Pd(II)complex had moderate activity against Candida albicans and strong activity against Saccharomyces cerevisiae. The Ni(II) complex had strong efficacy against every fungal organism tested except Candida albicans, which is slightly affected. The Fe(II) complex had promising effectiveness against all organisms tested. Candida albicans and Saccharomyces cerevisiae were all significantly inhibited by Fe(II) complex. Compared to their uncoordinated counterparts, these compounds' metal (II) complexes exhibited significantly higher activity.

Table 6: Antifungal studies of HCBHDCS ligand and its metal complexes

Compound	Antifungal Activity (zone of inhibition) (mm)	
	C albican	***S. C.***
HCBHDCS	7	9
$Fe(CBHDCS)_2$	13	15
$Co(CBHDCS)_2$	14	12
$Ni(CBHDCS)_2$	19	17
$Pd(CBHDCS)_2$	22	18
$Cu(CBHDCS)_2$	12	0
$Zn(CBHDCS)_2$	0	0
$Cd(CBHDCS)_2$	18	13
$Hg(CBHDCS)_2$	15	19
$Mn(CBHDCS)_2$	12	13
Fluconazole	13	14

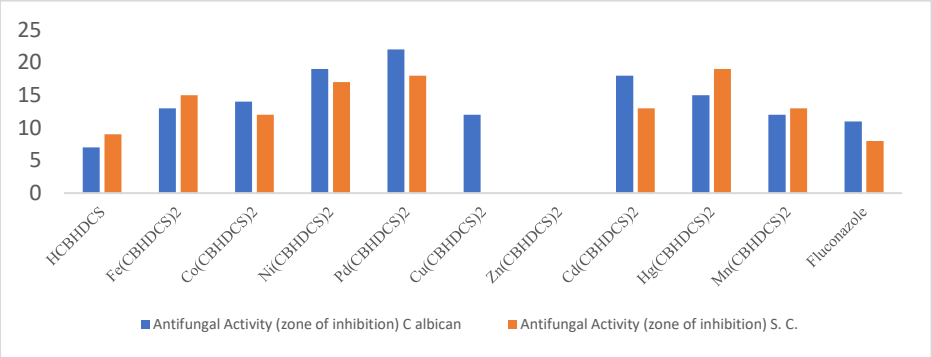

Figure 3: Antifungal activity of HCBHDCS ligand and its metal complexes

CYTOTOXIC STUDY:

All the synthesized compounds' cytotoxicity (brine shrimp bioassay) was tested according to the method developed by Meyer et al. [25]. As shown in **Table 7**, only three of the compounds tested, Pd(II), Mn(II), and Hg(II), exhibited significant cytotoxic action against Artemia salina, whereas the remaining compounds were largely inactive. The Hg(II) complex had the highest activity in this series (LD50 = 110mg/ml), while the HCBHDCS ligand demonstrated significantly lower activity (LD_{50} = 150µg/ml). It was also shown that coupling with metal ions reduced the cytotoxic characteristics of these molecules.

Table 7: Cytotoxic bioassay of HCBHDCS ligand and its metal complexes

Compound	LD_{50} (µg/ml)
HCBHDCS	150
Fe(CBHDCS)$_2$	130
Co(CBHDCS)$_2$	140
Ni(CBHDCS)$_2$	145
Pd(CBHDCS)$_2$	125
Cu(CBHDCS)$_2$	120
Zn(CBHDCS)$_2$	130
Cd(CBHDCS)$_2$	135
Hg(CBHDCS)$_2$	110
Mn(CBHDCS)$_2$	125

CONCLUSION:

Analytical, infrared (IR), electrical, magnetic, and electronic absorption spectra reached a comparable conclusion about ligand-metal bonding. This study determined that the HCBHDCS ligand had a monobasic tridentate structure concerning the transition metal ions Ferrous(II), cobalt(II), nickel(II), palladium(II), copper(II), cadmium(II), zinc(II), mercury(II), and manganese(II). Analytical and physicochemical research led to the assignment of octahedral geometry for the Fe(II), Co(II), Ni(II), Cu(II), and Mn(II) complexes, square planar geometry for Pd(II), and tetrahedral geometry for Zn(II), Cd(II), Hg(II), and Mn(II) complexes. The metal complexes have substantially more antibacterial activity than the ligand. The ligand and its complexes often exhibit significantly stronger activity than standard Streptomycin against E. coli bacteria. Complex structures are classified as such based on spectral analyses:

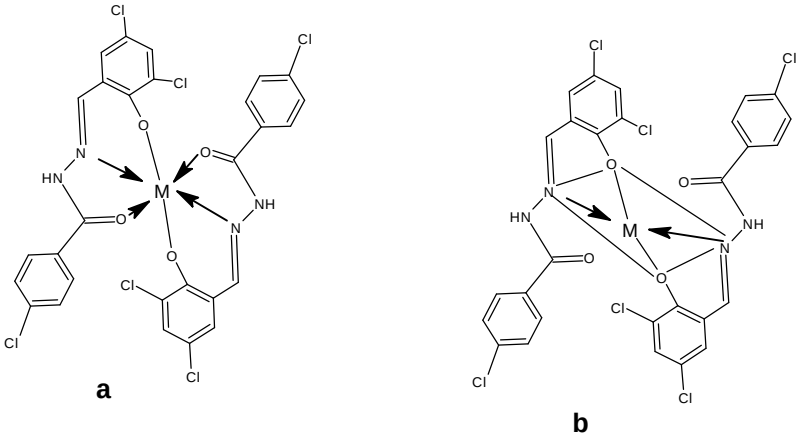

Where M = **a**) Fe(II), Mn(II), Co(II), Ni(II) and Cu(II) **b**) Pd(II), Cd(II), Hg(II) and Zn(II)

Figure 4: Structures of proposed metal complexes

REFERENCES:

1. Choi, T. S., & Tezcan, F. A. (2022). Design of a flexible, Zn-Selective protein Scaffold that displays anti-Irving–Williams Behavior. Journal of the American Chemical Society, 144(39), 18090-18100.
2. Andrezálová, L., & Országhová, Z. (2021). Covalent and noncovalent interactions of coordination compounds with DNA: An overview. Journal of Inorganic Biochemistry, 225, 111624.
3. Sigel, A., Sigel, H., Freisinger, E., & Sigel, R. K. (Eds.). (2018). Metallo-drugs: development and action of anticancer agents. De Gruyter.
4. Franz, K. J., & Metzler-Nolte, N. (2019). Introduction: Metals in medicine. Chemical Reviews, 119(2), 727-729.
5. Ghosh, S. (2019). Cisplatin: The first metal-based anticancer drug. Bioorganic chemistry, 88, 102925.
6. Karges, J., Stokes, R. W., & Cohen, S. M. (2021). Metal complexes for therapeutic applications. Trends in Chemistry, 3(7), 523-534.
7. Kovács, R., & Majoros, L. (2020). Fungal quorum-sensing molecules: A review of their antifungal effect against Candida biofilms. Journal of Fungi, 6(3), 99.
8. Chandra S., Vandana, and Kumar S., (2015). Synthesis, spectroscopic, anticancer, antibacterial and antifungal studies of Ni(II) and Cu(II) complexes with hydrazine carboxamide, 2-[3-methyl-2- thienyl methylene], Spectrochimica Acta Part A: Molecular and Biomolecular Spectroscopy, vol. 135, pp. 356–363.
9. Han, X., Lv, W., Guo, S. Y., Cushman, M., & Liang, J. H. (2015). Synthesis and structure–activity relationships of novel 9-oxime acetylides with improved bactericidal activity. Bioorganic & Medicinal Chemistry, 23(19), 6437-6453.
10. El-Sharief, M. A. S., Abbas, S. Y., El-Sharief, A. M. S., Sabry, N. M., Moussa, Z., El-Messery, S. M., ... & El Sayed, M. T. (2019). 5-Thioxoimidazolidine-2-one derivatives: Synthesis, anti-inflammatory activity, analgesic activity, COX inhibition assay, and molecular modelling study. Bioorganic Chemistry, 87, 679-687.
11. López-Mejía, A., Ortega-Pérez, L. G., Magana-Rodriguez, O. R., Ayala-Ruiz, L. A., Pinón-Simental, J. S., Hernández, D. G., & Rios-Chavez, P. (2021). Protective effect of Callistemon citrinus on oxidative stress in rats with 1, 2-dimethylhydrazine-induced colon cancer. Biomedicine & Pharmacotherapy, 142, 112070.
12. Azam, F., Chaudhry, B. A., Ijaz, H., & Qadir, M. I. (2019). Caffeoyl-β-d-glucopyranoside and 1, 3-dihydroxy-2-tetracosanoylamino-4-(E)-nonadecene isolated from Ranunculus muricatus exhibit antioxidant activity. Scientific Reports, 9(1), 15613.
13. Zhang, Q., Dong, J., Cui, J., Huang, G., Meng, Q., & Li, S. (2018). Cytotoxicity of synthesized 1, 4-naphthoquinone oxime derivatives on selected human cancer cell lines. Chemical and Pharmaceutical Bulletin, 66(6), 612-619.
14. Kodama, M., & Kodama, T. (1982). Influence of corticosteroid hormones on the therapeutic efficacy of cyclophosphamide. Gann= Gan, 73(4), 661-666.
15. Osmaniye, D., Levent, S., Karaduman, A. B., Ilgın, S., Özkay, Y., & Kaplancıklı, Z. A. (2018). Synthesis of new benzothiazole acylhydrazones as anticancer agents. Molecules, 23(5), 1054.
16. Dai, H., Chen, J., Li, G., Ge, S., Shi, Y., Fang, Y., & Ling, Y. (2017). Design, synthesis, and bioactivities of novel oxadiazole-substituted pyrazole oximes. Bioorganic & Medicinal Chemistry Letters, 27(4), 950-953.
17. El-Tabl, A. S., Abd-El Wahed, M. M., El-Azm, M. I. A., & Faheem, S. M. (2020). Newly Designed Metal-based Complexes and their Cytotoxic Effect on Hepatocellular Carcinoma, Synthesis and Spectroscopic Studies. Journal of Chemistry and Chemical Sciences, 10(1), 10-31.
18. Jassem, A. M., Mohammed, M. Q., Alharis, R. A., Jabir, H. A., & Alzearah, I. N. (2020). Study of adduct compounds between oxovanadium complexes VO (IV) and some biological relevance using FTIR technique. Chemical Papers, 74, 1087-1102.
19. Damena, T., Alem, M. B., Zeleke, D., Desalegn, T., Eswaramoorthy, R., & Demissie, T. B. (2022). Synthesis, characterization, and biological activities of zinc (II), copper (II) and nickel (II) complexes of an aminoquinoline derivative. Frontiers in Chemistry, 10, 1053532.
20. Borges, L. J., Bull, E. S., Fernandes, C., Horn Jr, A., Azeredo, N. F., Resende, J. A., ... & Kanashiro, M. M. (2016). In vitro and in vivo studies of the antineoplastic activity of copper (II) compounds against human leukaemia THP-1 and murine melanoma B16-F10 cell lines. European journal of medicinal chemistry, 123, 128-140.
21. Vogel AI. A Text Book of Quantitative Inorganic Analysis. 4th Edition. London: Longman ELBS;(1978), p 439.
22. Bain, G. A., & Berry, J. F. (2008). Diamagnetic corrections and Pascal's constants. Journal of Chemical Education, 85(4), 532.
23. El-Gammal, O. A., Mohamed, F. S., Rezk, G. N., & El-Bindary, A. A. (2021). Structural characterization and biological activity of new metal complexes based on Schiff base. Journal of Molecular Liquids, 330, 115522.
24. Abu-Khadra, A. S., Farag, R. S., & Abdel-Hady, A. E. D. M. (2016). Synthesis, characterization and antimicrobial activity of Schiff base (E)-N-(4-(2-hydroxybenzylideneamino) phenylsulfonyl) acetamide metal complexes. American Journal of Analytical Chemistry, 7(03), 233.
25. Meyer, B. N., Ferrigni, N. R., Putnam, J. E., Jacobsen, L. B., Nichols, D. E. J., & McLaughlin, J. L. (1982). Brine shrimp: a convenient general bioassay for active plant constituents. Planta medica, 45(05), 31-34.
26. Russell, R. M., & Robertson, J. L. (1979). Programming probit analysis. Bulletin of the ESA, 25(3), 191-193.
27. Paruch, K., Popiołek, Ł., Biernasiuk, A., Hordyjewska, A., Malm, A., & Wujec, M. (2020). Novel 3-Acetyl-2, 5-disubstituted-1, 3, 4-oxadiazole: Synthesis and biological activity. Molecules, 25(24), 5844.
28. Plant, N. (2004). Strategies for using in vitro screens in drug metabolism. Drug Discovery Today, 9(7), 328-336.
29. Şenol, D., & Kaya, İ. (2017). Synthesis and characterization of azomethine polymers containing ether and ester groups. Journal of Saudi Chemical Society, 21(5), 505-516.
30. Ross-Medgaarden, E. I., & Wachs, I. E. (2007). Structural determination of bulk and surface tungsten oxides with UV− vis diffuse reflectance and Raman spectroscopy. The Journal of Physical Chemistry C, 111(41), 15089-15099.
31. Dragna, J. M., Pescitelli, G., Tran, L., Lynch, V. M., Anslyn, E. V., & Di Bari, L. (2012). In situ assembly of octahedral Fe (II) complexes for the enantiomeric excess determination of chiral amines using circular dichroism spectroscopy. Journal of the American Chemical Society, 134(9), 4398-4407.
32. McCaffery, A. J., Stephens, P. J., & Schatz, P. N. (1967). Magnetic, optical activity of d-d transitions. Octahedral chromium (III), cobalt (III), cobalt (II), nickel (II), and manganese (II) complexes. Inorganic Chemistry, 6(9), 1614-1625.
33. Selwood, P. W. (2013). Magnetochemistry. Read Books Ltd.
34. Li, Y. J., Guo, S. Z., Feng, T., Xie, K. F., & Dong, W. K. (2021). An investigation into three-dimensional octahedral multi-nuclear Ni (II)-based complexes supported by a more flexible salami-type ligand. Journal of Molecular Structure, 1228, 129796.
35. Li, L. L., Feng, S. S., Zhang, T., Wang, L., & Dong, W. K. (2022). Counteranion-solvent-dependent construction of two octahedral homopolynuclear Ni (II) complexes with a symmetrical multi-halogen-substituted bis (salamo)-based ligand. Inorganica Chimica Acta, 534, 120815.
36. Chai, L. Q., Tang, L. J., Chen, L. C., & Huang, J. J. (2017). Structural, spectral, electrochemical and DFT studies of two mononuclear manganese (II) and zinc (II) complexes. Polyhedron, 122, 228-240.
37. Bon, V. V., Orysyk, S. I., Pekhnyo, V. I., & Volkov, S. V. (2010). Square-planar 1: 2 Ni (II) and Pd (II) complexes with different coordination modes of salicylaldehyde (4)-phenylthiosemicarbazone: Synthesis, structure and spectral properties. Journal of Molecular Structure, 984(1-3), 15-22.

38. Nnabuike, G. G., Salunke-Gawali, S., Patil, A. S., Butcher, R. J., & Obaleye, J. A. (2020). Synthesis and structures of tetrahedral zinc (II) complexes bearing indomethacin and nitrogen donor ligands. Inorganica Chimica Acta, 513, 119941.
39. Shaker, S. A., Khaledi, H., Cheah, S. C., & Ali, H. M. (2016). New Mn (II), Ni (II), Cd (II), and Pb (II) complexes with 2-methyl benzimidazole and other ligands. Synthesis, spectroscopic characterization, crystal structure, magnetic susceptibility, and biological activity studies. Arabian journal of chemistry, 9, S1943-S1950.
40. Łuczkowski, M., Padjasek, M., Ba Tran, J., Hemmingsen, L., Kerber, O., Habjanič, J., ... & Krężel, A. (2022). An Extremely Stable Interprotein Tetrahedral Hg (Cys) 4 Core Forms in the Zinc Hook Domain of Rad50 Protein at Physiological pH. Chemistry–A European Journal, 28(66), e202202738.
41. Preserova, J., Ranc, V., Milde, D., Kubistova, V., & Stavek, J. (2015). Study of phenolic profile and antioxidant activity in selected Moravian wines during the winemaking process by FT-IR spectroscopy. Journal of Food Science and Technology, 52, 6405-6414.
42. Sani, S., Kurawa, M. A., & Siraj, I. T. (2018). Solid state synthesis, spectroscopic, and x-ray studies of cu(ii) Schiff base complex derived from 2-hydroxy-3-methoxybenzaldehyde and 1, 3-phenylenediamine. Chem Search Journal, 9(1), 76-82.
43. Smith, B. C. (2017). The carbonyl group, part I: introduction. Spectroscopy, 32(9), 31-36.
44. Máirtin, Ó., Astill, C., & Schumm, S. (2003). Potentiometric, FTIR and NMR studies of the complexation of metals with theaflavin. Dalton Transactions, (5), 801-807.
45. Vojta, D., & Vazdar, M. (2014). The study of hydrogen bonding and π··· π interactions in phenol··· ethynylbenzene complex by IR spectroscopy. Spectrochimica Acta Part A: Molecular and Biomolecular Spectroscopy, 132, 6-14.
46. Mohan, P. K., Sreelakshmi, G., Muraleedharan, C. V., & Joseph, R. (2012). Water soluble complexes of curcumin with cyclodextrins: Characterization by FT-Raman spectroscopy. Vibrational Spectroscopy, 62, 77-84.
47. Alhazmi, H. A. (2019). FT-IR spectroscopy for identifying binding sites and measurements of the binding interactions of important metal ions with bovine serum albumin. Scientia Pharmaceutica, 87(1), 5.
48. Kang, L., Zhang, M., Liu, Z. H., & Ooi, K. (2007). IR spectra of manganese oxides with either layered or tunnel structures. Spectrochimica Acta Part A: Molecular and Biomolecular Spectroscopy, 67(3-4), 864-869.
49. Bushiri, M. J., Antony, C. J., & Fleck, M. (2008). Raman and infrared spectral studies of [C (NH2) 3] 2MII (H2O) 4 (SO4) 2, MII= Mn, Cd and VO. Journal of Raman Spectroscopy: An International Journal for Original Work in all aspects of Raman Spectroscopy, Including Higher Order Processes, and Brillouin and Rayleigh Scattering, 39(3), 368-373.
50. Thompson, M. C., Ramsay, J., & Weber, J. M. (2017). Interaction of CO2 with atomic manganese in the presence of an excess negative charge probed by infrared spectroscopy of [Mn (CO2)n]− clusters. The Journal of Physical Chemistry A, 121(40), 7534-7542.
51. Gautam, C., Yadav, A. K., & Singh, A. K. (2012). A review on infrared spectroscopy of borate glasses with effects of different additives. ISRN ceramics, 1-17.
52. Černý, R., Penin, N., Hagemann, H., & Filinchuk, Y. (2009). The first crystallographic and spectroscopic characterization of a 3 d-metal borohydride: Mn (BH4) 2. The Journal of Physical Chemistry C, 113(20), 9003-9007.
53. Stylianou, M., Drouza, C., Viskadourakis, Z., Giapintzakis, J., & Keramidas, A. D. (2008). Synthesis, structure, magnetic properties, and aqueous solution characterization of p-hydroquinone and phenol iminodiacetate copper (II) complexes. Dalton Transactions, (44), 6188-6204.
54. Karadeniz, Ş., Ataol, C. Y., Özen, T., Demir, R., Öğütçü, H., & Bati, H. (2019). Synthesis, characterization, and biological activities of Ni (II), Cu (II) and UO2 (VI) complexes of N'-((2Z, 3E)-3-(hydroxyimino) butan-2-ylidene)-2-phenylacetohydrazide. Journal of Molecular Structure, 1175, 39-48.
55. Gampp, H., Haspra, D., Maeder, M., & Zuberbuehler, A. D. (1984). Copper (II) complexes with linear pentadentate chelators. Inorganic Chemistry, 23(23), 3724-3730.
56. Iskander M.F., Sayed L. El, Salem N. M. H., Werner R., and Haase W.,(2003).Metal complexes derived from hydrazoneoxime ligands: I. Synthesis, characterization and magnetochemical studies of (acylhydrazoneoxime) copper(II) complexes. Journal of Coordination Chemistry, Journalvol. 56, no. 12, pp. 1075–1084.
57. Kivelson, D., & Neiman, R. (1961). ESR studies on the bonding in copper complexes. The Journal of Chemical Physics, 35(1), 149-155.
58. Karlin, K. D., & Tyeklár, Z. (2012). Bioinorganic chemistry of copper. Springer Science & Business Media.
59. Potterat, O., & Hamburger, M. (2006). Natural products in drug discovery concepts and approaches for tracking bioactivity. Current Organic Chemistry, 10(8), 899-920.
60. Plant, N. (2004). Strategies for using in vitro screens in drug metabolism. Drug Discovery Today, 9(7), 328-336.
61. Dar, O. A., Lone, S. A., Malik, M. A., Wani, M. Y., Ahmad, A., & Hashmi, A. A. (2019). New transition metal complexes with a pendent indole ring: insights into the antifungal activity and mode of action. *RSC advances*, *9*(27), 15151-15157.

DOI: https://doi.org/10.15379/ijmst.v10i5.3638